Comparison of RADARSAT-2 and Sentinel-1 DInSAR displacements over upland ice-wedge polygonal terrain, Banks Island, Northwest Territories, Canada

N.H. Short and R.H. Fraser

2023

Canada

GEOMATICS CANADA
OPEN FILE 73

Comparison of RADARSAT-2 and Sentinel-1 DInSAR displacements over upland ice-wedge polygonal terrain, Banks Island, Northwest Territories, Canada

N.H. Short and R.H. Fraser

2023

Permanent link: https://doi.org/10.4095/331683

This publication is available for free download through GEOSCAN (https://geoscan.nrcan.gc.ca/).

Publications in this series have not been edited; they are released as submitted by the author.

Summary

Comparisons of ground displacement measurements from RADARSAT-2 and Sentinel-1 Differential Interferometric Synthetic Aperture Radar (DInSAR) data show that high resolution RADARSAT-2 data (1-2 m) can distinguish differential thaw settlement patterns between ice-wedge troughs and polygon centres. Medium resolution Sentinel-1 data (~20 m) cannot distinguish ground displacements over these smaller scale permafrost landforms. In addition, the medium resolution DInSAR data tend to under-estimate the true settlement of the ground, due to spatial averaging and the fact that smaller features with stronger subsidence trends are missed. High resolution ground displacement maps can be useful for infrastructure planning and engineering. Medium resolution displacement maps may be useful for regional scale overviews, trend detection and change monitoring.

Table of Contents

Table of Figures

1. Introduction

Differential Interferometric Synthetic Aperture Radar (DInSAR) is a well-proven technique for detecting movement of the Earth's surface using airborne and spaceborne radar sensors (Gabriel et al., 1989; Massonnet and Feigl, 1995 and 1998). DInSAR measures the phase difference in the radar line-of-sight (LOS) direction between pairs of repeat radar acquisitions. These phase differences are essentially distance differences and can be used to measure movement of the ground away from or toward the radar sensor (Gabriel et al., 1989). Longer periods of time can be observed and accuracy levels improved by using multiple pairs or stacks of repeat SAR acquisitions (Sandwell and Price, 1998). In permafrost terrain, ground movement or displacement, is due to seasonal freeze and thaw of the active layer, long term degradation or aggradation of permafrost, and local slope and geomorphological processes (e.g. solifluction, creep and slumping). DInSAR has been applied to monitor ground displacement in permafrost terrain with broad success for more than a decade (e.g. Liu et al., 2010; Short et al., 2011; Short et al., 2014; Daout et al., 2017; Strozzi et al., 2018; Rudy et al., 2018; Chen et al., 2018; Antonova et al., 2018; Rouyet et al., 2019). The technique has become an integral part of studying the short- and long-term dynamics of permafrost landscapes (e.g. Liu et al., 2015; Schaefer et al., 2015; Chen et al., 2020; Rouyet et al., 2021; Zwieback and Meyer, 2021; Wang et al., 2023).

In permafrost terrain, the displacement associated with geomorphological features varies depending on their material composition and ice content. Geomorphological features also vary widely in size. Large-scale features can be eskers, bedrock outcrops, saturated soil areas, pingos, and areas of patterned ground that are typically 10s to 100s of metres, even kilometres in size. Small-scale features can be ice-wedge cracks and troughs, individual tundra polygons, frost blisters, palsas, lithalsas, and pockets of organic material within a bedrock feature. These features are more on the scale of decimetres, metres and 10s of metres. The spatial resolution of the radar sensor will dictate the periglacial features that can be detected in a DInSAR map of ground displacement. The level of detail contained in a DInSAR displacement map will determine whether it is useful for regional trend detection, local trends and general planning, or whether it has sufficient information to identify specific features, to potentially infer the causes of local displacement patterns and thus be useful for site planning and engineering.

RADARSAT-2 is a C-band SAR satellite launched in 2007 and operated by MacDonald Dettwiler and Associates. The satellite has a 24 day repeat cycle and offers a variety of imaging

modes, including a Spotlight mode with 1 m spatial resolution. This Spotlight mode has been shown to be valuable for detailed study of permafrost terrain with results that can be useful at the site planning and engineering level (Short et al., 2014). RADARSAT-2 data are commercial though, so must be ordered, have high expense and limited archive availability. Sentinel-1 is a constellation of C-band SAR satellites launched by the European Space Agency, beginning in 2014. Systematic SAR observations are acquired every 12 days, providing extensive data stacks for DInSAR analysis. Sentinel-1 data are free and open, hence it is relatively easy and highly desirable to use them. The nominal spatial resolution for Sentinel-1 Interferometric Wide Swath mode is ~20 m.

High resolution RADARSAT-2 data have been used extensively and successfully over the past decade by the Government of Canada (GoC) as a source of terrain stability information for permafrost regions. As the availability of RADARSAT-2 data to the GoC shifts and replacement sources of terrain stability information are sought, it is important to understand the potential and limitations of the different data sources. This short report compares the information content of high resolution RADARSAT-2 and medium resolution Sentinel-1 DInSAR data over a permafrost area with distinctive periglacial landforms. Banks Island in Arctic Canada has extensive upland polygons with ice-wedge troughs dissecting the landscape. The trough features are 1-5 m in width and the polygons vary from 20 - 200 m. We use DInSAR data from the two satellite systems to illustrate the level of detail in periglacial features that can be detected.

2. Banks Island study site

Banks Island, Northwest Territories, is undulating glaciated terrain, underlain by continuous, cold, ice-rich permafrost (Vincent, 1982; England et al., 2009; French, 2017). The eastern side of the island is characterized by Jesse Till and the Amundsen Moraine, an ice cored moraine deposit from the Late Wisconsinan glaciation (England et al., 2009). The area is mapped as extensive ground ice (O'Neill et al., 2022). Upland surfaces can be quite barren, but vegetation is present in depressions and sheltered areas and is generally small and low-growing. Arctic willow, sedges, herbs, moss and lichen are present, and noticeably more lush in depressions and along water courses where moisture is retained (Fraser et al., 2018). The lack of thermal buffering from vegetation or an organic layer is thought to closely link the active layer response to summer warming (Fraser et al., 2018; Farquharson et al., 2019). Thaw depths on northeastern Banks Island have been measured to reach 120 cm (Farquharson et al., 2019).

Figure 1. Location of Banks Island in Canada's Northwest Territories. Blue square is the study site. Red triangle is Sachs Harbour.

The small, 40 km^2, study area is located slightly inland on the southeast of the island (72°05'40"N, 120°48'18"W) (blue square in Figure 1). The area is characterised by large, upland ice-wedge polygon areas interspersed with waterbodies and water courses (Figure 2). These upland ice-wedge polygons are experiencing widespread, warming-induced, ice-wedge degradation and the development of thermokarst and ponding (Rudy et al., 2017; Fraser et al., 2018; Farquharson et al., 2019). The ice-wedges of Banks Island are known to be large, potentially exceeding 3 m wide and 10 m deep (French, 1974), resulting in dramatic thermokarst when melting occurs. Long-term settlement of <60 cm over 12 years has been measured in polygonal terrain on northeastern Banks Island and is attributed to the melting of ice-wedges (Farquharson et al., 2019).

Figure 2. A) Aerial photograph of upland polygonal landscape of eastern Banks Island. B) Photograph of polygonal terrain, with vegetation and ponding in an ice-wedge trough. C) Panchromatic Worldview-2 image from 31 July, 2017, with 0.5 m spatial resolution. Scale bar indicates the size of the polygons and the interconnecting ice-wedge troughs. The location of the Worldview-2 focus area is shown in Figure 3. Photos courtesy of GNWT.

3. Data

3.1 SAR data

SAR acquisitions from 2019 were used for the analysis. Table 1 lists the RADARSAT-2 and Sentinel-1 DInSAR stack characteristics.

Table 1. SAR acquisitions

Data set	Acquisition dates (yyyymmdd)	Beam mode and polarization	Multi-looking ratio and output pixel spacing (m) SR-Slant range GR-Ground range	Satellite look direction (° from North)	Mid-scene incidence angle (°)
RADARSAT-2					
Ascending	20190612 20190706 20190730 20190823	Spotlight 23 HH	1 x 3 1.3 x 1.2 SR 1.8 x 1.2 GR	80.5	46.7
Sentinel-1A/B					
Descending	20190703 20190715 20190727 20190808 20190820* 20190901	IW3 HH	4 x 1 9.3 x 13.8 SR 13.6 x 13.8 GR 8 x 2 18.6 x 27.6 SR 27.2 x 27.6 GR	296.2	43.4

Sentinel-1 reference scene. Note that RADARSAT-2 used a reference scene from a preceding summer stack that is not discussed here (20180828).

Data sets stop at the end of August or in very early September to avoid early freeze up and ground heave which causes loss of coherence and movement that would detract from the summer subsidence trend.

The SAR data sets have opposing look directions with RADARSAT-2 being ascending and Sentinel-1 descending. This is not ideal but is a limitation of what is available in the satellite archives. The low slope terrain and the omnidirectional nature of the polygons mitigates this limitation.

Both sensors are C-band and incidence angles are similar, ~47° for RADARSAT-2 and ~43° for Sentinel-1, which minimizes differences in results due to sensor parameters other than resolution and look direction.

3.2 Ancillary data

High resolution elevation data are necessary to derive intricate patterns of ground displacement reliably from DInSAR, otherwise subtle geomorphological details are obscured by residual topographic phase errors (Short et al., 2009). For Banks Island the 2 m ArcticDEM Version 3.0 was used (Porter et al., 2018). Figure 3A shows the elevation range for the study area and Figure 3B shows the local slopes. In general, the study area is quite flat, most slopes are < 5°, so slope processes would not be expected in the three month time frame. In flat areas any movement can be expected to be largely vertical, so results should be similar in ascending and descending data. Only in the southeast corner are slopes more significant (5 - 15°). Because the RADARSAT-2 ascending data have a line-of-sight that is west to east, whereas the Sentinel-1 descending data have a line-of-sight that is east to west, here the displacement patterns could be conflicting. To minimize this limitation, the detailed analysis of spatial resolution impacts focuses on an area of very low slopes (< 3°) outlined by a box in Figure 3.

A Worldview-2, 0.5 m resolution, panchromatic image from 31 July, 2017 was used for visual comparisons with the DInSAR results.

Waterbody polygons at 1:50,000 scale were obtained from the topographic data portal of Natural Resources Canada (https://atlas.gc.ca/toporama/en/index.html).

Sachs Harbour is the closest community to the study area (152 km to the west, Figure 1) and intermittent weather data are collected there. The Mean Annual Air Temperature at Sachs Harbour is -12.8°C (Environment Canada, 2022a). The 1981-2010 July and August daily average air temperatures were 6.6 and 3.7°C respectively, but in 2019 the July and August daily averages were only 3.9 and 2.3°C (Environment Canada, 2022b), therefore 2019 was considered to be a cool summer. Precipitation rates are unfortunately not reliably measured so we do not know if 2019 was a wet, dry, or average summer.
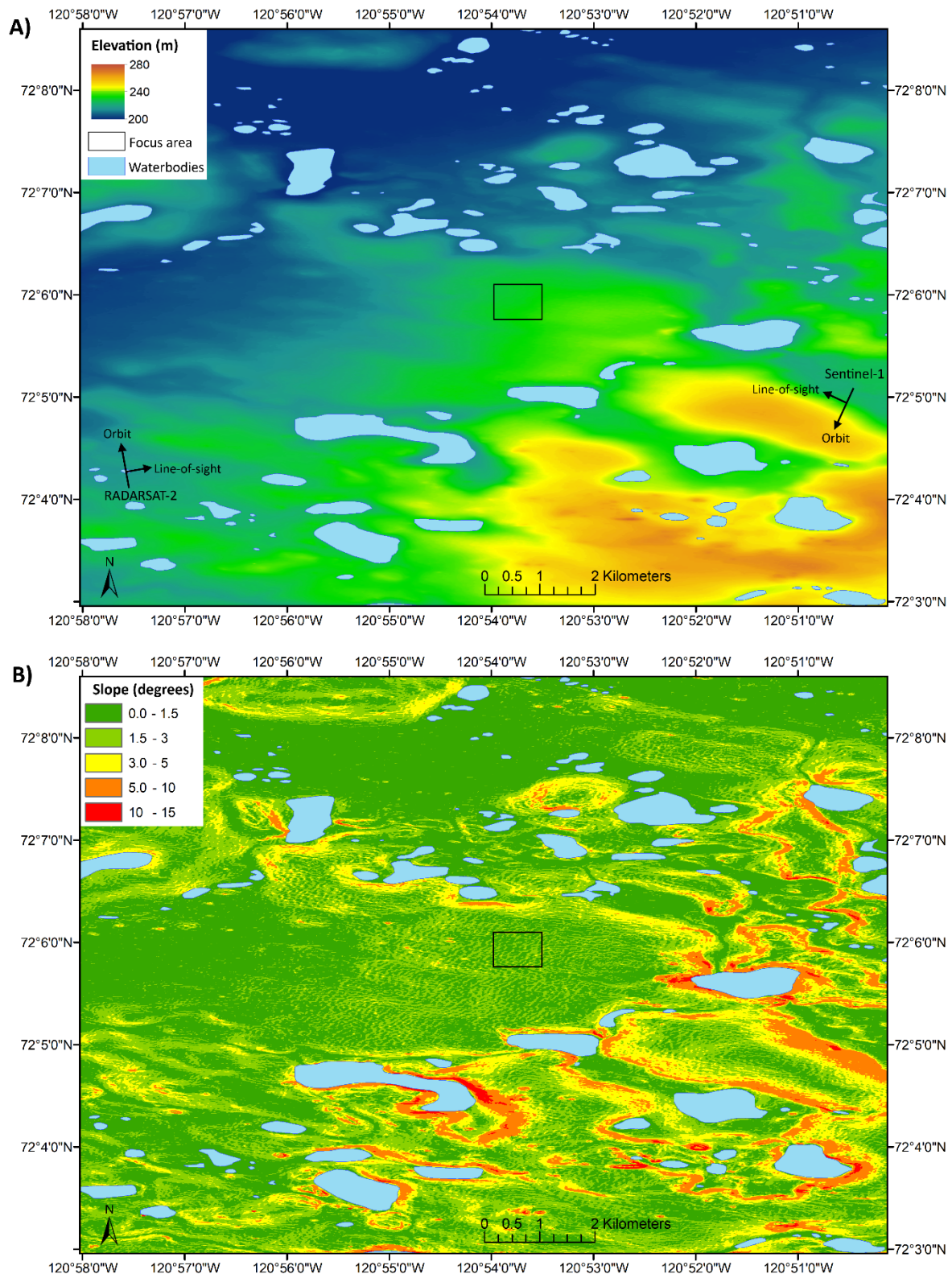
Figure 3. A) Elevation range for the Banks Island study area from the 2 m ArcticDEM. B) Local slopes derived from the ArcticDEM

4. Method

The DInSAR processing was accomplished using the GAMMA software (GAMMA, 2019). Processing followed the conventional steps of SAR image co-registration to a single reference, interferogram formation, topographic phase removal using an external DEM, phase filtering (Goldstein and Werner, 1998), phase unwrapping (Costantini, 1998) and large-scale phase trend removal. All possible interferograms were formed within the summer stacks but interferograms were visually inspected and those with significant coherence loss or atmospheric noise were removed from the processing. The phase unwrapping proceeded from a single reference point identified as bedrock, thus calibrating all the displacements to this stable point (green star in Figure 4). The location of bedrock was provisionally identified based on fringe patterns in interferograms and confirmed with optical imagery. Unwrapped interferograms were stacked and the seasonal displacement trend was derived from the inputs according to the equation given in Short et al. (2014). The displacements are visualised as movement in the sensor line-of-sight.

Multi-looking is common practice in radar analysis because when the data are processed at full resolution the resulting product suffers from what is termed speckle noise. Multi-looking averages the processed data, reducing the speckle noise in both the imagery and the phase measurements. The multi-looking ratios used in the processing are given in Table 1. The multi-looking ratios were chosen to obtain an approximately square pixel, in either slant or ground range, to keep the data averaging to a bare minimum and to preserve as much detail as possible. Sentinel-1 data were processed with two multi-looking ratios to explore information content. The Sentinel-1 SAR nominal spatial resolution is 20 m. The product pixel spacings are such that multi-looking ratios can be chosen to be either slightly oversampled, to give ~15 m pixels, or slightly undersampled to give ~25 m pixels (varying slightly with beam position), but it is not possible to get exactly 20 m. The Sentinel-1 data were thus processed twice, once with 4 x 1 multi-looking, delivering output products with ~14 m pixels and once with 8 x 2 multi-looking, yielding ~27 m pixels (ground range).

As mentioned, the RADARSAT-2 data are ascending while the Sentinel-1 data are descending. This would be expected to produce reverse trends in the observations, except that the terrain is generally quite flat. In flat terrain displacement tends to be only in the vertical direction and vertical subsidence would record as movement away from the sensor whichever the path direction. Where there are slopes, those facing the sensor may see a subdued signal, as downward movement away from the sensor would be offset by horizontal movement toward the sensor. Downslope movement on slopes facing away from the sensor would record as strong

line-of-sight lengthening, as both downward and horizontal movement would be movement away from the sensor.

5. Results

5.1 RADARSAT-2

Figure 4 shows the overview results from the RADARSAT-2 DInSAR processing. Stable areas are cream or pale yellow in colour, indicating displacement values of < 1 cm. 1 cm has been found to be a good practical approximation of the noise in DInSAR data, below which the displacement signal is considered to be negligible (Short et al., 2014). The stable areas are typically exposed bedrock and include the area where the DInSAR reference point is located. Red colours indicate significant subsidence and highlight the ice-wedge troughs between the upland polygons, several linear features aligned with drainage channels in the centre west (DC), and patches of greater subsidence close to waterbodies.
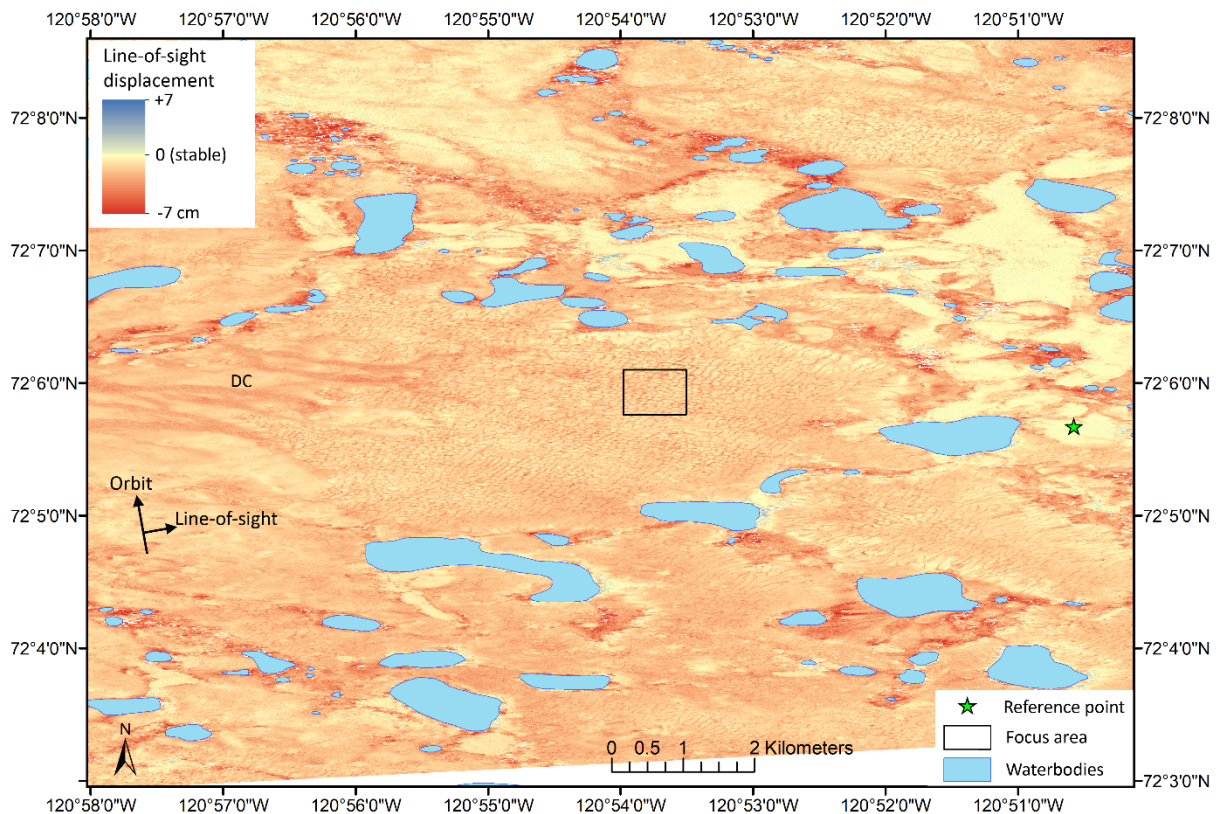

Figure 4. Seasonal line-of-sight displacement in 2019 derived from RADARSAT-2 data over the Banks Island study site. Negative values (red) are movement downward or away from the satellite. Positive values (blue) are movement upward or toward the satellite. DC indicates area with drainage channels.

5.2 Sentinel-1 with 4 x 1 multi-looking

Figure 5 shows the 4 x 1 multi-looking result for Sentinel-1 over the same area. Pale yellow stable areas often coincide with the RADARSAT-2 result although the shapes of the areas are not as clearly defined and there is more variability (noise) in the Sentinel-1 measurements. A mottled texture is apparent over the areas of upland polygons but the polygons themselves are not clearly defined. The network of drainage channels (DC) visible in the west of the RADARSAT-2 result is also present in the Sentinel 4 x 1 result, although not as clearly defined. In general, the subsidence patterns are comparatively subdued. In the southwest corner of the image some patches of stability and low displacements are observed in the high resolution RADARSAT-2 result but these are not clearly defined in the Sentinel 4 x 1 result nor as consistent in direction. Subtle movement toward the Sentinel radar may be a result of small slope features and the directionality of the SAR in this area, but phase drift with distance from the reference point could also be an issue as there is a general trend of stronger displacements in the north and lower displacements in the south compared to the RADARSAT-2 result.

Figure 5. Seasonal line-of-sight displacement in 2019 derived from Sentinel-1 with 4 x 1 multi-looking over the Banks Island study site. Negative values (red) are movement downward or away from the satellite. Positive values (blue) are movement upward or toward the satellite. DC indicates area with drainage channels.

5.3 Sentinel-1 with 8 x 2 multi-looking

Figure 6 shows the displacement results achieved using the Sentinel-1 data with 8 x 2 multi-looking. Comparable areas of stability are visible but the patterns are much less defined. Some general areas of subsidence can be seen near waterbodies but the first gaps in the data, due to loss of coherence, are also visible. Very subtle mottling is apparent over the upland polygon areas but it is not obvious that there are polygons and it would be hard to identify without prior knowledge of the landscape. The drainage channels in the west part of the map (DC) are also there in trace amounts, but again, would be hard to interpret without other knowledge of the area. As with the 4 x 1 result, there is a slight trend of higher displacements in the north than in the south and the southwest corner has some slightly positive displacement values suggesting movement toward the sensor.
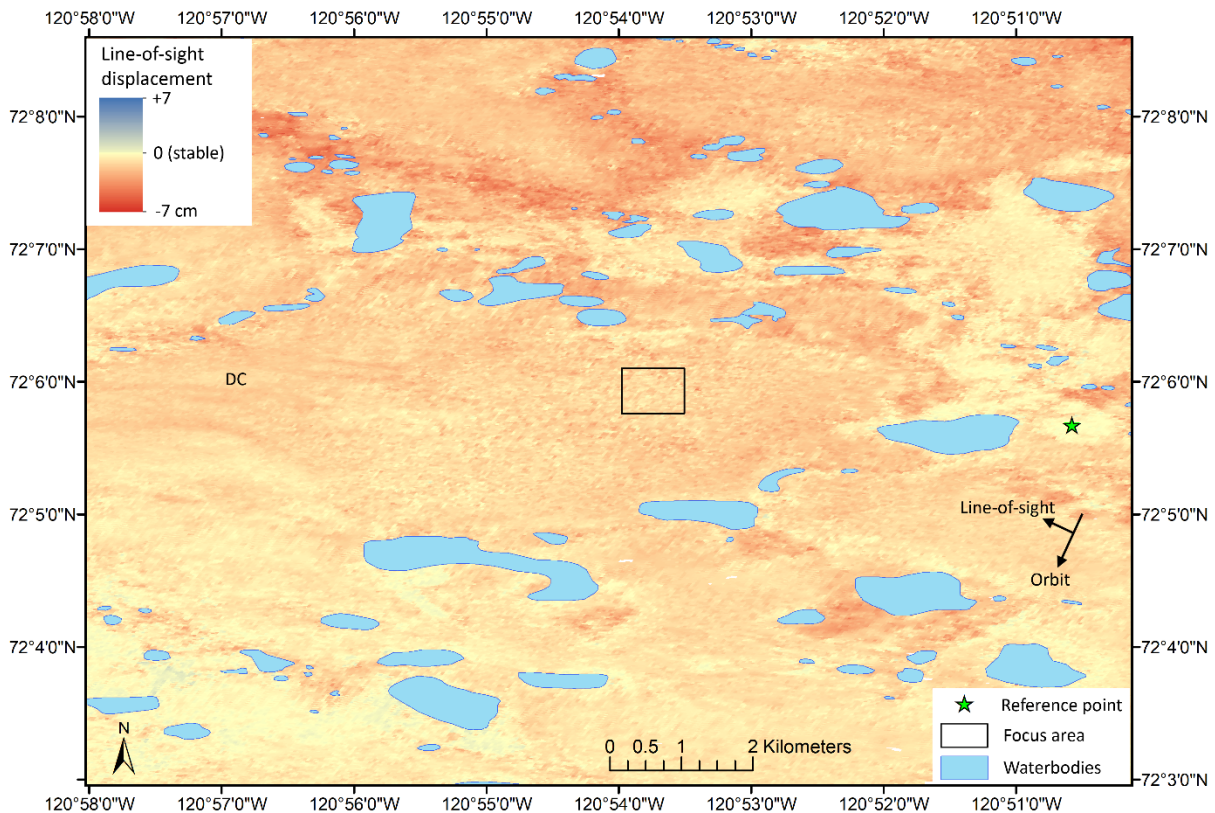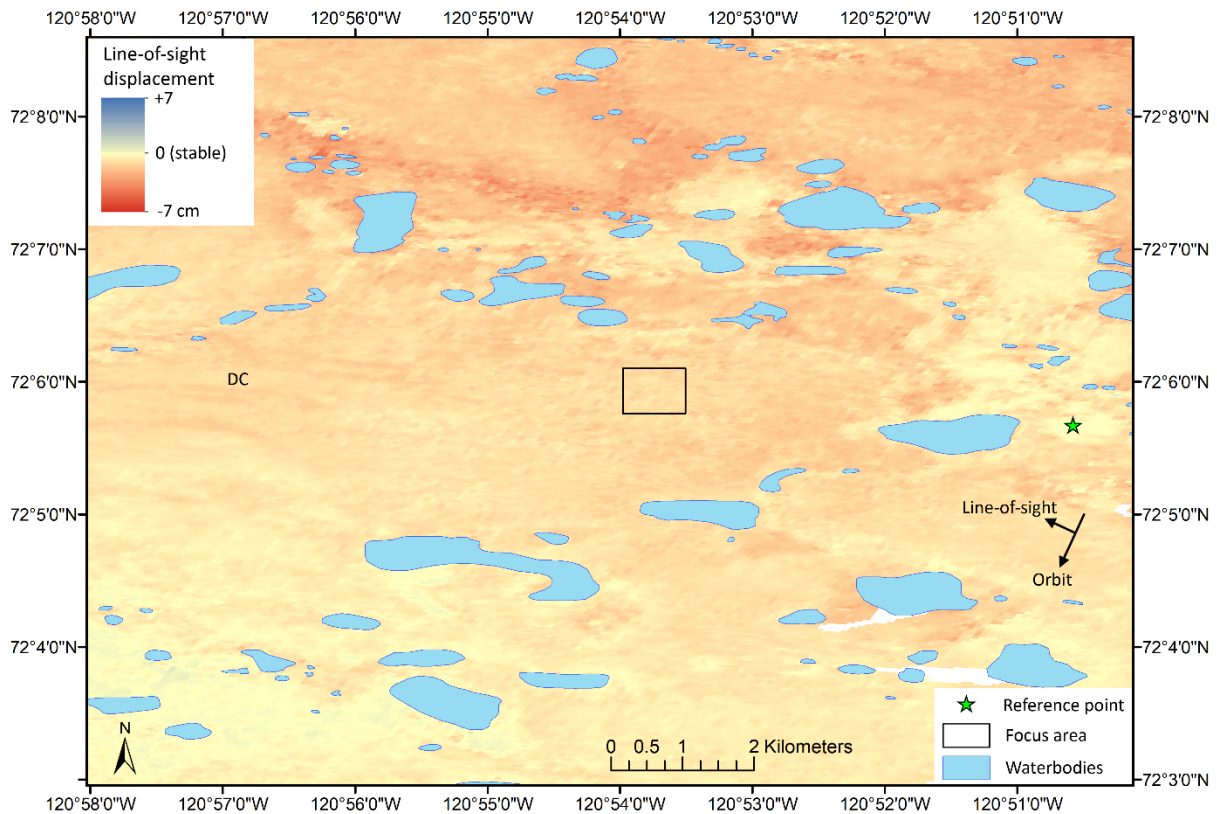

Figure 6. Seasonal line-of-sight displacement in 2019 derived from Sentinel-1 with 8 x 2 multi-looking over the Banks Island study site. Negative values (red) are movement downward or away from the satellite. Positive values (blue) are movement upward or toward the satellite. White areas indicate 'no data' due to loss of coherence. DC indicates area with drainage channels.

5.4 Polygon focus area and displacement distribution

Figure 7 shows the focus area of the upland polygons for the three data sets. The difference in level of detail is striking. The polygons are clearly visible in the RADARSAT-2 displacements but the polygons are not discernable in either the 4 x 1 (~14 m) or the 8 x 2 (~27 m) Sentinel-1 data. Although the patterned ground gives a mottled texture in the Sentinel-1 overview data sets, the individual polygons are not discernable in the focus area.

One last observation is that the distribution of the displacement measurements varies as a function of the resolution of the data. The pixel displacements for the polygon focus area are plotted in Figure 8. This isolated focus area is used specifically to avoid any discrepancies due to different data extents, the inclusion of unreliable waterbody values and to minimize slope and directionality effects. It is apparent that there are thousands more pixels in the RADARSAT-2 coverage than the Sentinel-1 which is expected. Slightly less expected is the dramatic reduction in the range of measured displacements. RADARSAT-2 displacements have a range of ~9 cm. Sentinel-1 with 4 x 1 multi-looking have a range of ~5 cm. With 8 x 2 multi-looking the Sentinel-1 range reduces to less than 2 cm. Statistically this is not a surprise, but it has important implications for the fidelity with which medium resolution DInSAR results could ever be expected to match with ground truth measurements, and how much confidence should be ascribed to Sentinel-1 measurements of ground displacement.
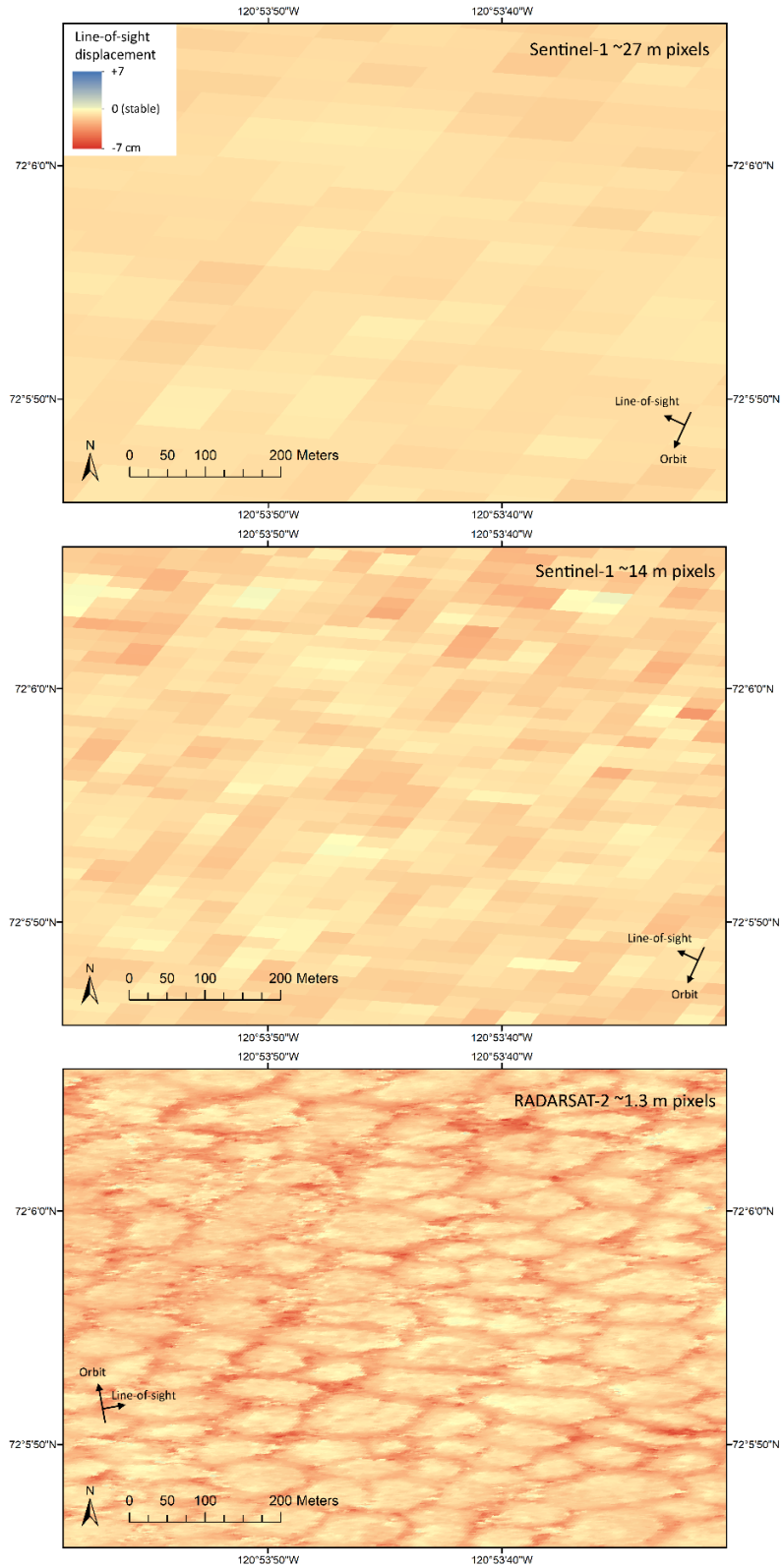
Figure 7. Focus area of ice-wedge polygons and seasonal line-of-sight displacements measured by Sentinel-1 and RADARSAT-2. Corresponding high resolution panchromatic image is shown in Figure 2C. Location of the focus area is shown in Figure 3.
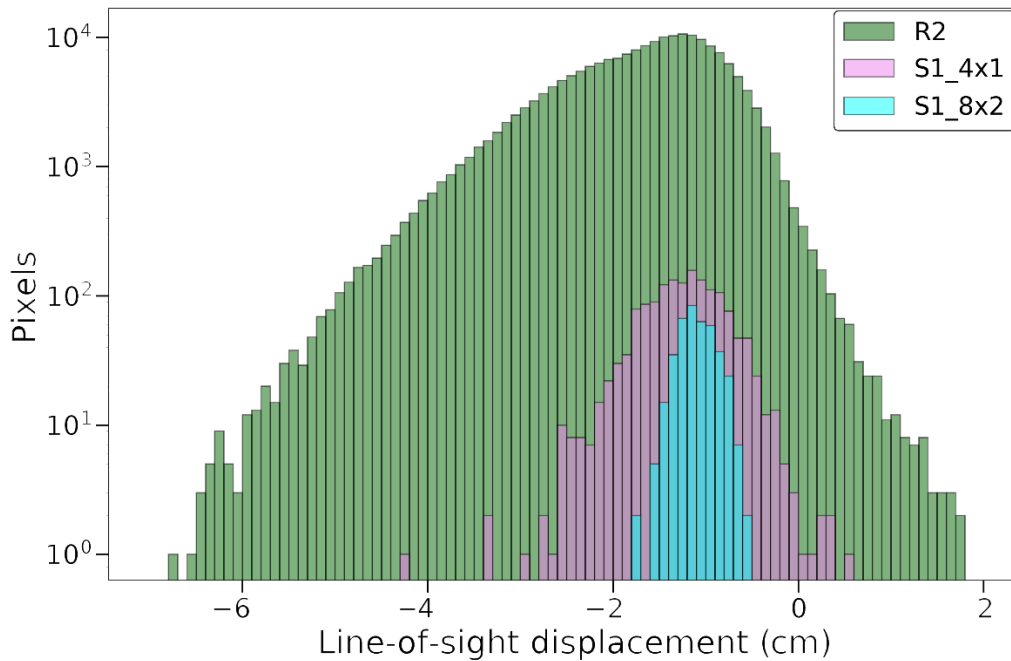
Figure 8. Histogram of seasonal line-of-sight displacements measured by RADARSAT-2 (R2) and Sentinel-1 (S1) over the polygon focus area.

6. Discussion

In high resolution (<1-2 m) DInSAR data sets, ice-wedge troughs, polygons and detailed geomorphological features can be clearly seen, due to their different properties, ice contents, and distinct thaw settlement behaviours. These features are not visible in the medium resolution (10-30 m) data sets, although general areas of displacement trends can be discerned. Being able to discern individual landforms is a key factor in determining what a displacement map can be useful for. From an engineering perspective it can be good practise to avoid building on ice-wedges, to place building pilings in mounds between ice-wedges, or to dig out ice-wedges and/or back fill troughs with thaw insensitive materials (Jones et al., 2022). Very detailed maps of ground displacement with individual features can therefore aid in planning construction. In addition, connections and relationships between subsidence features can help to understand surface and subsurface water flows, and can inform engineering mitigation measures or simply avoidance (Short et al., 2014). In contrast, the medium resolution data cannot provide enough detail to inform decision making at a local scale, they provide only general overviews as to stable and less stable areas. These polygonal terrain results agree with other authors who have

concluded that the spatial resolution of Sentinel-1 InSAR subsidence observations is insufficient to distinguish differential subsidence within ice-wedge polygons (Zwieback and Meyer, 2021), and more generally, that the 'high sub-pixel spatial variability of ground movements' must be considered when interpreting DInSAR results in permafrost environments (Antonova et al., 2018). In the medium resolution data sets, processing with the lowest appropriate multi-looking ratios can help to preserve texture, which helps to separate landscape units even if individual landforms cannot be detected.

In addition, the histogram in Figure 8 clearly shows that the Sentinel-1 data with lower spatial resolution do not capture the full range of ground displacement. If we project the line-of-sight displacements to vertical using the satellite geometry, which would be more appropriate for comparing with in-situ measurements, RADARSAT-2 captured subsidence down to -10 cm, Sentinel-1 with 4 x 1 multi-looking captured to -4.5 cm, and 8 x 2 multi-looking captured to -2.5 cm. From field measurements we know that thaw settlement rates much greater than -2.5 cm are common in permafrost terrain and related to the ice content and depth of the active layer (e.g. Tarnocai et al., 2004), therefore the medium resolution data are almost certainly missing some of the settlement of the ground. A thaw settlement rate of -3.5 cm for an active layer of <130 cm would be characteristic of ice-poor sediments with dry, coarse-grained geology (Oldenborger et al., 2022). Therefore, the medium resolution data are likely missing the settlement associated with ice-rich features that subside at higher rates, because they are smaller than the pixel resolution and are averaged away and missed. In this case, the relatively narrow ice-wedge troughs are missed. Quantitative conclusions from Sentinel-1 data about subsidence in permafrost terrain will therefore be inherently limited by the fact that medium resolution data tend to under-estimate settlement rates, even with the bare minimum of multi-looking applied. This will be an inherent limitation whenever comparing medium resolution DInSAR measurements with field measurements and when incorporating DInSAR measurements into algorithms or mathematical models of permafrost terrain and behaviour.

The medium resolution data also seem to be more susceptible to phase drift from the reference point. Whether it is a limitation of the phase trend correction method used here, or whether because the phase values do not track the true displacement of the ground as faithfully, over long distances the unwrapped phase values tend to diverge further from reality. This could perhaps be mitigated by using more than one reference point as was done here.

6.1 Sources of error

Variations in soil moisture content are now well understood to affect DInSAR phase measurements (Zwieback et al., 2017). Increasing soil wetness will cause line-of-sight lengthening which registers as movement away from the sensor or downward subsidence. Conversely, drying of the ground causes line-of-sight shortening, apparent as movement toward the sensor or uplift (Zwieback et al., 2015). The soil moisture signal is small though, estimated to be ~1/8th of the radar wavelength (Zwieback et al., 2015). In the C-band data here, Sentinel-1 and RADARSAT-2 should be similarly affected and soil moisture should not contribute more than ~0.7 cm of spurious signal. As the displacement measurements in the high resolution data have a range of <8 cm, the majority of the signal should be displacement of the ground, although this error becomes a larger proportion of the displacement signal in the medium resolution data with their limited range.

Vegetation growth can also cause errors in DInSAR measurements as plant moisture levels decrease as plants mature, causing drying and an uplift signal (Zwieback and Hajnsek, 2016). This is thought to be ~1 cm in shrubs (Zwieback and Meyer, 2021), however, in the extremely low biomass environment of the polygonal terrain of Banks Island, this would likely be much less.

Flooding of the ground and the accumulation of surface water can cause either coherence loss or, if the flooded area is small enough to preserve pixel coherence, then likely noise in the signal. If the ground continues to subside under a consistently flooded surface the result would be an underestimation of the true ground subsidence (Short et al., 2014), but if water levels fluctuate there would be no relationship between seasonal phase trends and ground subsidence. Less reliable displacement measurements might therefore be expected in areas with surface ponding.

7. Conclusion

This report shows that highly detailed information about ground displacement within small-scale permafrost terrain features can be derived using high resolution DInSAR data. This example of differential thaw subsidence within ice-wedge polygons is made possible by the Spotlight mode of RADARSAT-2. This level of detail can be useful for infrastructure and engineering planning. It will not replace the need for geotechnical investigations but it can certainly guide initial assessments, provisional building locations and strategies, and help with deciding where to locate more detailed fieldwork.

Sentinel-1 medium resolution DInSAR data may be useful for regional trends and long-term assessment and observation, but small-scale features such as ice-wedges, polygons, palsas and lithalsas will not be reliably detected. The large-scale coverage of the data may make them useful for regional scale preliminary assessments for infrastructure, but the results need to be interpreted with caution. In addition, there is a tendency for the true displacement of the ground to be under-estimated in medium resolution data due to spatial averaging. This has implications for modelling and true representation of terrain dynamics. Medium resolution DInSAR data may benefit from additional reference areas or calibration points to correct for phase drift over large distances.

The limitations of medium resolution Sentinel-1 data would also apply to the RADARSAT Constellation Mission (RCM) 16M and 30M beam modes. The advantages of the Spotlight mode would apply to the RCM Spotlight mode and potentially the RCM Very High Resolution 3 m mode as well.

8. Acknowledgments

9. References

Antonova, S., Sudhaus, H., Strozzi, T., Zwieback, S., Kääb, A., Heim, B., Langer, M., Bornemann, N., and Boike, J. (2018). Thaw subsidence of a Yedoma landscape in northern Siberia, measured in situ and estimated from TerraSAR-X interferometry. *Remote Sensing*, 10(4): 494. doi:10.3390/rs10040494

Chen, J., Günther, F., Grosse, G., Liu, L. and Lin, H. (2018). Sentinel-1 InSAR Measurements of Elevation changes over Yedoma Uplands on Sobo-Sise Island, Lena Delta. *Remote Sensing*, 10(7): 1152. doi:10.3390/rs10071152

Chen J., Wu, Y., O'Connor, M., Cardenas, M. B., Schaefer, K., Michaelides, R. and Kling, G. (2020). Active layer freeze-thaw and water storage dynamics in permafrost environments inferred from InSAR. *Remote Sensing of Environment*, 248:112007 https://doi.org/10.1016/j.rse.2020.112007

Costantini, M. (1998). A novel phase unwrapping method based on network programming. *IEEE Transactions on Geoscience and Remote Sensing*, 36(3): 813-821. doi: 10.1109/36.673674.

Daout, S., Doin, M.-P., Peltzer, G., Socquet, A. and Lasserre C. (2017). Large-scale InSAR monitoring of permafrost freeze-thaw cycles on the Tibetan Plateau. *Geophysical Research Letters*, 44, doi:10.1002/2016GL070781

Ecosystem Classification Group (2013). *Ecological Regions of the Northwest Territories— Northern Arctic*; Department of Environment and Natural Resources, Government of the Northwest Territories: Yellowknife, NT, Canada. https://www.geomatics.gov.nt.ca/en/services/web-mapping-applications/forest-management-divisions-fmd-ecosystem-classification-photo-map

England J.H., Furze, M. and Doupé, J. (2009). Revision of the NW Laurentide Ice Sheet: implications for paleoclimate, the northeast extremity of Beringia and Arctic Ocean sedimentation. *Quaternary Science Reviews*, 28: 1573-96.

Environment Canada (2022a). https://climate.weather.gc.ca/climate_normals/results_1981_2010_e.html [Accessed Nov 4, 2022]

Environment Canada (2022b) https://climate.weather.gc.ca/historical_data/search_historic_data_e.html. [Accessed, Nov 4, 2022].

Farquharson, L. M., Romanovsky, V. E., Cable, W. L., Walker, D. A., Kokelj, S. V. and Nicolsky, D. (2019). Climate change drives widespread and rapid thermokarst development in

very cold permafrost in the Canadian High Arctic. *Geophysical Research Letters*, 46: 6681-6689. doi:101029/2019GL082187

Fraser, R. H., Kokelj, S. V., Lantz, T. C., McFarlane-Winchester, M., Olthof, I., and Lacelle, D. (2018). Climate sensitivity of high Arctic permafrost terrain demonstrated by widespread ice-wedge thermokarst on Banks Island. *Remote Sensing*, 10(6): 954-978. doi:10.3390/rs10060954

French, H. M. (1974). Active Thermokarst Processes, Eastern Banks Island, Western Canadian Arctic. *Canadian Journal of Earth Sciences*, 11: 785-794.

French, H. M. (2017). The Banks Island Tundra. In *Landscapes and Landforms of Western Canada*; *World Geomorphological Landscapes*. Springer: Cham, Switzerland: p.97-108. ISBN 978-3-319-44593-9.

Gabriel, A.K., Goldstein, R.M. and Zebker, H.A. (1989). Mapping small elevation changes over large areas: differential radar interferometry. *Journal of Geophysical Research*, 94(B7): 9183-9191.

GAMMA (2019) GAMMA Software Information v1.6, https://www.gamma-rs.ch/uploads/media/GAMMA_Software_information_02.pdf, 12 pages, [Accessed: 24 April, 2020].

Goldstein, R. M. & Werner, C. L. (1998). Radar interferogram filtering for geophysical applications. *Geophysical Research Letters*, 25(21), 4035–4038.

Jones, B., Peirce, J., Connor, B., Kanevskiy, M., Shur, Y., Curry, T., Bolz, P., and Tracey, B. (2022). Infrastructure and Permafrost Degradation in Point Lay, Alaska. *Witness the Arctic - Community Highlights,* September 27, 2022, Arctic Research Consortium of the United States. https://www.arcus.org/witness-the-arctic/2022/9/highlight/2

Liu, L., Schaefer, K., Chen, A., Gusmeroli, A., Zebker, H., and Zhang, T. (2015). Remote sensing measurements of thermokarst subsidence using InSAR. *Journal of Geophysical Research-Earth*, 120: 1935-1948.

Liu, L., Zhang, T. and Wahr, J. (2010). InSAR measurements of surface deformation over permafrost on the North Slope of Alaska. *Journal of Geophysical Research*, 115: F03023, doi:10.1029/2009JF001547

Massonnet, D. and Feigl, K., (1995). Discrimination of geophysical phenomena in satellite radar interferograms. *Geophysical Research Letters*, 22: 1537-1540

Massonnet, D., and Feigl, K. (1998). Radar interferometry and its application to changes in the Earth's surface. *Reviews of Geophysics*, 36: 441-500

Oldenborger, G. A, Short, N. and LeBlanc, A., (2022). Permafrost thaw sensitivity prediction using surficial geology, topography, and remote-sensing imagery: a data-driven neural network approach. *Canadian Journal of Earth Sciences*, 59: 897-913. dx.oi.org/10.1139/cjes-2021-0117

O'Neill, H. B., Wolfe, S. A. and Duchesne, C. (2022). Ground ice map of Canada; Geological Survey of Canada, Open File 8713, (ver. 1.1), 1 .zip file. https://doi.org/10.4095/330294

Porter, C., Morin, P., Howat, I., Noh, M-J., Bates, B., Peterman, K., Keesey, S., Schlenk, M., Gardiner, J., Tomko, K., Willis, M., Kelleher, C., Cloutier, M., Husby, E., Foga, S., Nakamura, H., Platson, M., Wethington, M. Jr., Williamson, C., Bauer, G., Enos, J., Arnold, G., Kramer, W., Becker, P., Doshi, A., D'Souza, C., Cummens, P., Laurier, F. and Bojesen, M. (2018). ArcticDEM, *https://doi.org/10.7910/DVN/OHHUKH*, Harvard Dataverse, V1, [Accessed: 28 Jan., 2020].

Rouyet, L., Liu, L., Strand, S. M., Christiansen, H. H., Lauknes, T.R., and Larsen, Y. (2021). Seasonal InSAR displacements documenting the active layer freeze and thaw progression in central-western Spitzbergen, Svalbard. *Remote Sensing*, 13(15). doi: 10.3390/rs13152977

Rouyet, L., Rune Lauknes, T., Christiansen, H., Strand, S. and Larsen, Y. (2019). Seasonal dynamics of a permafrost landscape, Adventdalen, Svalbard, investigated by InSAR. *Remote Sensing of Environment*, 231: 111236. doi:10.1016/j.rse.2019.111236

Rudy, A. C. A., Lamourex, S. F., Kokelj, S. V., Smith, I. R. and England, J. H. (2017). Accelerating thermokarst transforms ice-cored terrain triggering a downstream cascade to the ocean. *Geophysical Research Letters*, 44: 11,080 -11,087. doi: 10.1002/2017GL074912

Rudy, A., Lamoureux, S., Treitz, P., Short, N. and Brisco, B. (2018). Seasonal and multi-year surface displacements measured by DInSAR in a High Arctic permafrost environment. *International Journal of Applied Earth Observation and Geoinformation*, 64: 51–61. https://doi.org/10.1016/j.jag.2017.09.002

Sandwell, D. and Price, E. (1998). Phase gradient approach to stacking interferograms, *Journal of Geophysical Research*, 103(B12): 30,183-30,204. doi:10.1029/1998JB900008

Schaefer, K., Liu, L., Parsekian, A., Jafarov, E., Chen, A., Zhang, T., Gusmeroli, A., Panda, S., Zebker, H., and Schaefer, T. (2015). Remotely Sensed Active Layer Thickness (ReSALT) at Barrow, Alaska using Interferometric Synthetic Aperture Radar. *Remote Sensing*, 7: 3735-3759. doi:10.3390/rs70403735

Short, N., Brisco, B., Budkewitsch, P., and Murnaghan, K. (2009). ALOS-PALSAR Interferometry for Permafrost Monitoring in Canada. Proceedings of the 3rd ALOS PI Symposium, November 9-13, 2009, Big Island, Hawaii. Alaska SAR Facility, Fairbanks, Alaska

Short, N., Brisco, B., Couture, N., Pollard, W., Murnaghan, K. and Budkewitsch, P. (2011). A Comparison of TerraSAR-X, RADARSAT-2 and ALOS-PALSAR Interferometry for Monitoring Permafrost Environments, Case Study from Herschel Island, Canada, *Remote Sensing of Environment*, 115: 3491–3506. doi:10.1016/j.rse.2011.08012

Short, N., LeBlanc, A.-M., Sladen, W., Oldenborger, G., Mathon-Dufour, V. and Brisco, B. (2014). RADARSAT-2 D-InSAR for ground displacement in permafrost terrain, validation from Iqaluit Airport, Baffin Island, Canada. *Remote Sensing of Environment*, 141: 40-51, doi: 10.1016/j.rse.2013.10.016

Strozzi, T., Antonova, S., Günther, F., Mätzler, E., Vieira, G., Wegmüller, U., Westermann, S. and Bartsch, A. (2018). Sentinel-1 SAR interferometry for surface deformation monitoring in low-land permafrost areas. *Remote Sensing*, 10: 1360; doi:10.3390/rs10091360

Tarnocai, C., Nixon, F. M. and Kutney, L. (2004). Circumpolar-Active-Layer-Monitoring (CALM) Sites in the Mackenzie Valley, Northwestern Canada. *Permafrost and Periglacial Processes*, 15: 141-153. doi: 10.1002/ppp.490

Vincent, J.-S. (1982). The Quaternary History of Banks Island, N.W.T., Canada. *Géographie physique et Quaternaire*, 36(1-2): 209-232. doi:https://doi.org/10.7202/032478ar

Wang, L., Zhao, L., Zhou, H., Liu, S., Hu, G., Li, Z., Wang, C. and Zhao, J. (2023). Evidence of ground ice melting detected by InSAR and in situ monitoring over permafrost terrain on the Qinghai-Xizang (Tibet) Plateau. *Permafrost and Periglacial Processes*, 34(1): 52-67. doi:10.1002/ppp.2171

Zwieback, S. and Hajnsek, I. (2016). Influence of vegetation growth on the polarimetric DInSAR phase diversity – implications for deformation studies. *IEEE Transactions on Geoscience and Remote Sensing*, 54(5): 3070-3082.

Zwieback, S., Hensley, S., and Hajnsek, I. (2015). Assessment of soil moisture effects on L-band radar interferometry, *Remote Sensing of Environment*, 164: 77–89

Zwieback, S., Hensley, S., and Hajnsek, I. (2017). Soil moisture estimation using differential radar interferometry: Toward separating soil moisture and displacements. *IEEE Transactions on Geoscience and Remote Sensing*, 55(9): 5069-5083. doi: 10.1109/TGRS.2017.2702099.

Zwieback, S., and Meyer, F. J. (2021). Top-of-permafrost ground ice indicated by remotely sensed late-season subsidence. *The Cryosphere*, 15(4): 2041-2055.